

dues, as well as neuraminidase and *O*-glycosidase (Fig. 4B). This modification was not observed when Kir3.1 (1 to 373)-FCYENE was retained in the ER by fusing it to the α_{2C} -adrenergic receptor COOH-terminal 14 amino acids (11, 13) (Fig. 4B), containing an RXR(R)-type retention and retrieval motif that could override the ER export signal (see below). Thus channels acquired this modification after exiting the ER, a process promoted by the FCYENE sequence.

The FCYENE sequence exerted a similar trafficking effect on Kv1.2, a voltage-gated potassium channel with little homology to Kir family members (Fig. 4C, top panels). Because coexpression with Kv β 2 improves cell-surface targeting of Kv1.2, Kv β 2 is believed to facilitate the folding and maturation of Kv1.2 in the ER (14). Not only did the FCYENE motif mimic Kv β 2 in promoting Kv1.2 surface expression, it also largely occluded the ability of Kv β 2 to further promote surface expression of the fusion protein (Fig. 4C, bottom). Considering the similarity of the effects of Kv β 2 and the FCYENE sequence, it will be interesting to determine whether the ability of Kv β 2 to promote Kv1.2 surface expression reflects improved Kv1.2 folding or the presence of an ER export sequence in Kv β 2.

We next tested whether FCYENE can alter the subcellular localization of proteins that are normally held in the ER by retention and retrieval. We examined Kir6.2 or GABA_BR1a (a subunit of G protein-coupled receptor for the neurotransmitter γ -aminobutyric acid). The latter is a nonchannel protein that exists as a monomer or dimer (15). Both proteins, when expressed alone in COS7 cells, remain in the ER via an RXR(R)-mediated retention and retrieval mechanism (15, 16). Although deleting RKR from Kir6.2 (Kir6.2 Δ 36) (16) or mutating RSRR in GABA_BR1a to ASRR (GABA_BR1a-ASRR) (15) resulted in an increase of surface expression, the majority of the protein was still in the ER 24 hours after transfection (Fig. 4D). Strong Golgi staining and further increase of the surface expression were observed when FCYENE was introduced to the COOH-terminus of Kir6.2 Δ 36 or GABA_BR1a-ASRR (Fig. 4D), but not wild-type Kir6.2 or GABA_BR1a. FCYENE increased the surface expression and surface currents of Kir6.2 Δ 36 proportionately (Fig. 4E), suggesting that it did not simply allow misfolded or misassembled channel proteins to escape from the ER. Thus FCYENE could not override the ER retention and retrieval caused by RXR(R) under our experimental conditions. Furthermore, in the absence of RXR(R) retention and retrieval signals, the bulk of Kir6.2 Δ 36 and GABA_BR1a-ASRR exited the ER very slowly, but their ER export could be enhanced by the introduction of an exogenous ER export signal.

The FCYENE motif is conserved in the Kir2 subfamily but is absent in Kir1.1 (10),

yet the COOH-terminus of Kir1.1 could substitute for that of Kir2.1 in promoting forward trafficking (Fig. 1B). Thus we explored whether the COOH-terminus of Kir1.1 also contained an ER export signal. Indeed, ER export and surface expression were achieved by adding just the last 19 amino acids (YD-NPNFVLSVEVDETDDTQM) of Kir1.1 to either Kir2.1 (1 to 374) (Fig. 4F, top) or Kir6.2 Δ 36. Alanine scanning mutagenesis indicated that mutating either of the EXD sequences or the upstream VLS sequence abolished the ER export effect (Fig. 4F, bottom). Furthermore, conservative mutations of the acidic residues (E to D or D to E) were also not tolerated.

Thus, we have shown that Kir1.1 and Kir2.1 contain distinct ER-to-Golgi forward-trafficking signals that do not appear to be required for channel folding, assembly, or gating, but that are essential for export of the channels from the ER. Ion channels such as Kir6.2 Δ 36 and Kv1.2 largely remain in the ER because of a lack of forward-trafficking signals, and their steady-state surface expression and the current levels can be greatly enhanced by fusion with an exogenous ER export signal. Our results reinforce the notion that signals like the DXE motif of VSV-G increase the ER export rate (7, 8), and further demonstrate the physiological significance of diacidic motifs. We have also shown that the flanking residues of diacidic motif are essential for ER export, and they are not limited to Tyr-based residues as previously suggested (8, 17). The variation of forward-trafficking signals in different potassium

channels presents one potential mechanism for differential regulation of surface channel numbers.

References and Notes

1. B. Hille, *Ionic Channels of Excitable Membranes* (Sinauer Associates, Sunderland, MA, ed. 2, 1992).
2. J. E. Rothman, *Cell* **50**, 521 (1987).
3. S. M. Hurtley, A. Helenius, *Annu. Rev. Cell Biol.* **5**, 277 (1989).
4. M. Mizuno, S. J. Singer, *Proc. Natl. Acad. Sci. U.S.A.* **90**, 5732 (1993).
5. W. E. Balch, J. M. McCaffery, H. Plutner, M. G. Farquhar, *Cell* **76**, 841 (1994).
6. M. J. Kuehn, J. M. Herrmann, R. Schekman, *Nature* **391**, 187 (1998).
7. N. Nishimura, W. E. Balch, *Science* **277**, 556 (1997).
8. C. S. Sevier, O. A. Weisz, M. Davis, C. E. Machamer, *Mol. Biol. Cell* **11**, 13 (2000).
9. Single-letter abbreviations for the amino acid residues are as follows: A, Ala; C, Cys; D, Asp; E, Glu; F, Phe; G, Gly; H, His; I, Ile; K, Lys; L, Leu; M, Met; N, Asn; P, Pro; Q, Gln; R, Arg; S, Ser; T, Thr; V, Val; W, Trp; and Y, Tyr.
10. C. G. Nichols, A. N. Lopatin, *Annu. Rev. Physiol.* **59**, 171 (1997).
11. Supplementary information is available on Science Online at www.sciencemag.org/cgi/content/full/291/5502/316/DC1.
12. M. E. Kennedy *et al.*, *J. Biol. Chem.* **274**, 2571 (1999).
13. B. Schwappach, N. Zerangue, Y. N. Jan, L. Y. Jan, *Neuron* **26**, 155 (2000).
14. G. Shi *et al.*, *Neuron* **16**, 843 (1996).
15. M. Margeta-Mitrovic, Y. N. Jan, L. Y. Jan, *Neuron* **27**, 97 (2000).
16. N. Zerangue, B. Schwappach, Y. N. Jan, L. Y. Jan, *Neuron* **22**, 537 (1999).
17. S. I. Bannykh, N. Nishimura, W. E. Balch, *Trends Cell Biol.* **8**, 21 (1998).
18. We thank J. Trimmer for the Kv β 2 cDNA and Y.-M. Chan, M. Margeta-Mitrovic, and other Jan lab members for comments on the manuscript. L.Y.J. and Y.N.J. are Howard Hughes Medical Institute Investigators.

12 October 2000; accepted 5 December 2000

Autoimmune Dilated Cardiomyopathy in PD-1 Receptor-Deficient Mice

Hiroyuki Nishimura,¹ Taku Okazaki,¹ Yoshimasa Tanaka,² Kazuki Nakatani,⁶ Masatake Hara,³ Akira Matsumori,³ Shigetake Sasayama,³ Akira Mizoguchi,⁴ Hiroshi Hiai,⁵ Nagahiro Minato,² Tasuku Honjo^{1*}

Dilated cardiomyopathy is a severe pathology of the heart with poorly understood etiology. Disruption of the gene encoding the negative immunoregulatory receptor PD-1 in BALB/c mice, but not in BALB/c RAG-2^{-/-} mice, caused dilated cardiomyopathy with severely impaired contraction and sudden death by congestive heart failure. Affected hearts showed diffuse deposition of immunoglobulin G (IgG) on the surface of cardiomyocytes. All of the affected PD-1^{-/-} mice exhibited high-titer circulating IgG autoantibodies reactive to a 33-kilodalton protein expressed specifically on the surface of cardiomyocytes. These results indicate that PD-1 may be an important factor contributing to the prevention of autoimmune diseases.

Dilated cardiomyopathy is a chronic disorder of the heart muscle characterized by a poorly contractile and dilated ventricle. The diagno-

sis is based primarily on clinical criteria and on the exclusion of identifiable underlying causes (1). Consequently, patients with dilated

REPORTS

ed cardiomyopathy represent a heterogeneous group affected to varying degrees by genetic, viral, immunological, and environmental factors (2). This has complicated identification of the underlying pathogenic mechanisms op-

erative in this disease. Involvement of an immune mechanism in patients with dilated cardiomyopathy is still controversial (3), although a certain fraction of patients do possess antibodies against self antigens (4–6).

We examined the potential contribution of an autoimmune pathway in a spontaneous model of dilated cardiomyopathy.

When bred on the BALB/c background (7), PD-1^{-/-} mice started to die as early as 5 weeks of age (Fig. 1A). By 30 weeks, two-thirds of PD-1^{-/-} and 10% of PD-1^{+/-} mice had died, whereas all of the PD-1^{+/+} controls survived. In contrast, premature death was not observed in either BALB/c PD-1^{-/-}–RAG2^{-/-} or B6–PD-1^{-/-} mice (8). Diseased PD-1^{-/-} mice exhibited protrusion of eyeballs a few weeks preceding death, and autopsy examination revealed that all diseased mice exhibited massively enlarged hearts (Fig. 1B) and varying degrees of hepatomegaly. Collectively, these features suggested that the cause of death was congestive heart failure. Histological examination (9) revealed that the right ventricular walls of PD-1^{-/-} mice were thinner than those of the control mice, and that both ventricles were dilated about twofold in diameter (Fig. 1C). Sporadic fibrotic reaction, including increased cellularity and interstitial fibrosis with scar formation (Fig. 1C, right), was also observed, although the ventricular walls appeared otherwise grossly normal, without any apparent infiltration of mononuclear cells. Electron microscopic examination (9), however, revealed the scattered degeneration of cardiomyocytes with disarrayed and disrupted myofilaments and irregularly shaped mitochondria throughout the ventricular walls [Fig. 1D and Web fig. 1 (10)].

To evaluate heart function, we performed transthoracic echocardiography (11) on diseased, as well as PD-1^{+/+} control, mice. Ventricular cavities of PD-1^{-/-} mice, in particular those of the right ventricles, appeared greatly dilated, and their wall thickness was markedly reduced as compared with those of PD-1^{+/+} mice (Fig. 2A, “2D”). The movement of cardiac walls of the left ventricle and interventricular septum was decreased at both diastole (LVdD) and systole (LVdS) in PD-1^{-/-} mice (Fig. 2A, “M-mode”), and the ventricular fractional shortening (11), a measure of systolic function, was greatly reduced, from 71.9% (PD-1^{+/+}) to 14.9% (PD-1^{-/-}) ($P < 0.005$) (Fig. 2B). These findings indicated that the pump function of the dilated hearts of PD-1^{-/-} mice was severely impaired in a manner consistent with dilated cardiomyopathy (12).

Fig. 1. Development of dilated cardiomyopathy in BALB/c–PD-1^{-/-} mice leading to heart failure. (A) Survival curves for PD-1^{+/+}, PD-1^{+/-}, PD-1^{-/-}, and PD-1^{-/-}–RAG2^{-/-} mice. (B) Representative images of hearts from PD-1^{+/+} (left) and PD-1^{-/-} (right) mice. (C) Hematoxylin and eosin staining of the mid-transverse section of hearts from PD-1^{+/+} (+/+) (left) and PD-1^{-/-} (-/-) (middle) shown at the same magnification. LV, left ventricle; RV, right ventricle. (Right) The ventricular region of PD-1^{-/-} mice (-/-) (original magnification, $\times 40$). Arrows indicate cellular proliferation, consisting mainly of fibroblasts. (D) Electron micrographs of hearts from PD-1^{+/+} (+/+) and PD-1^{-/-} (-/-) mice. Arrowheads indicate the degenerated cardiac myocyte apposed by the relatively intact ones. MF and Mc indicate myofilaments and mitochondria, respectively. Original magnification, $\times 8000$.

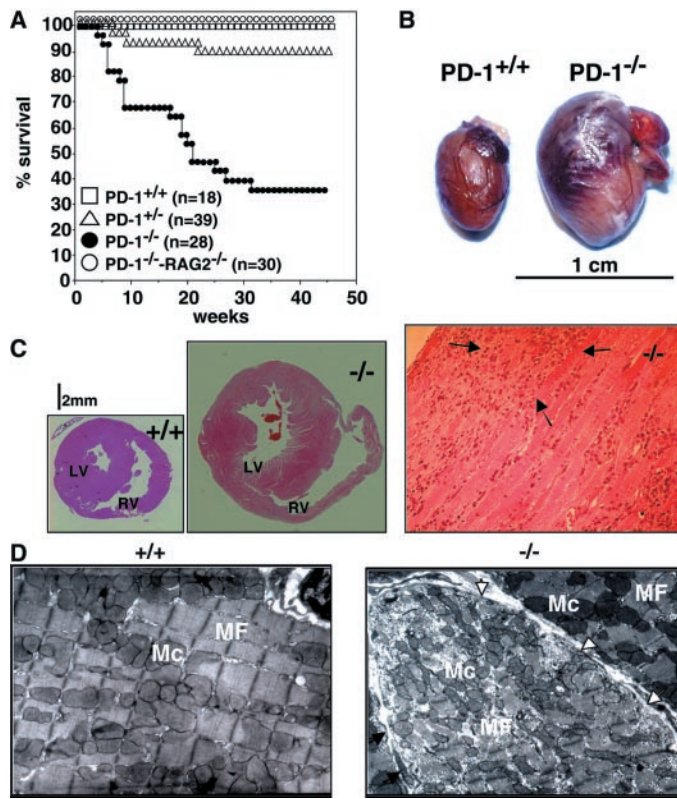
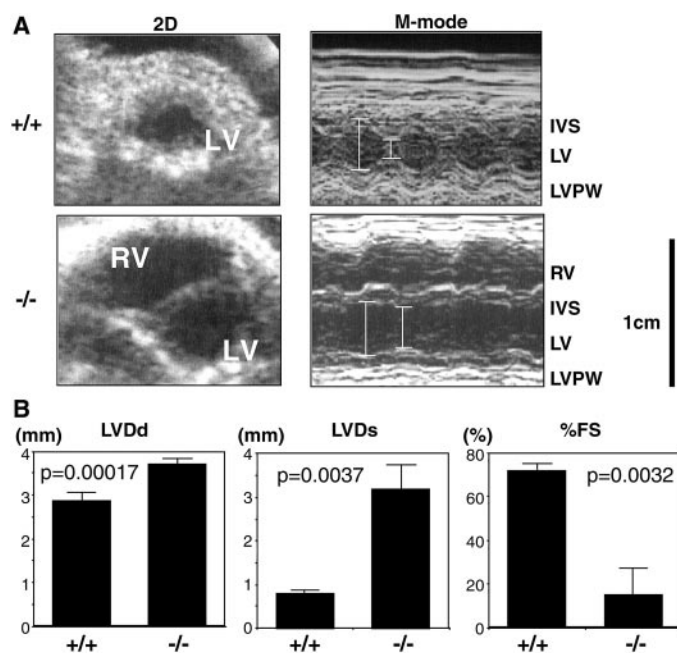


Fig. 2. Dilatation and impaired movement of hearts from PD-1^{-/-} mice as revealed by transthoracic echocardiography. (A) Echocardiographic analyses of heart from PD-1^{+/+} (upper) and PD-1^{-/-} (lower) mice. Representative images of 2D (left) and M-mode (right) analyses are shown (11). Bars in M-mode images indicate left ventricular end-diastolic (left) and end-systolic (right) dimensions. IVS, interventricular septum; LV, left ventricle; RV, right ventricle; LVPW, left ventricular posterior wall. (B) Indices of heart movement based on the echocardiographic analysis of PD-1^{+/+} ($n = 5$) and PD-1^{-/-} ($n = 4$) mice. LVdD, left ventricular end-diastolic dimension; LVdS, left ventricular end-systolic dimension; and %FS, percent fraction shortening. Statistical significance (P value) was evaluated by Student's t test.



¹Department of Medical Chemistry, ²Department of Immunology and Cell Biology, ³Department of Cardiovascular Medicine, ⁴Department of Anatomy and Neurobiology, ⁵Department of Pathology and Biology of Diseases, Graduate School of Medicine, Kyoto University, Yoshida Konoe-cho, Sakyo, Kyoto, 606-8501, Japan. ⁶Second Department of Anatomy, Osaka City University Medical School, 1-4-3 Asahi-Machi, Abeno-Ku, Osaka, 545-8585, Japan.

*To whom correspondence should be addressed. E-mail: honjo@mfour.med.kyoto-u.ac.jp

REPORTS

Because all PD-1^{-/-} mice bred on the BALB/c-RAG-2^{-/-} background remained healthy (Fig. 1A), we attributed development

of the heart disease in BALB/c-PD-1^{-/-} mice to the functions of T and/or B lymphocytes. Consistent with this notion, prelimi-

nary studies revealed that disease could be successfully transferred into RAG-2^{-/-} mice with spleen or bone marrow cells from diseased mice. In these experiments, recipient mice that developed cardiomyopathy again exhibited high-titer autoantibodies of equivalent specificity to those observed in the original animals (13). We therefore examined PD-1^{-/-} mice for signs of heart-specific immune reactions. Immunofluorescent analysis (9) revealed the linear deposition of immunoglobulin G (IgG), but little IgM, together with C3 complement surrounding the cardiomyocytes in the affected PD-1^{-/-} hearts, whereas no significant IgG deposition was detected in PD-1^{+/+} hearts (Fig. 3A). The isotype of the deposited IgG was predominantly IgG1 (14). IgG deposition was observed diffusely throughout the entire cardiac wall regardless of the presence of tissue damage. Little IgG deposition could be detected in other organs, including renal glomeruli (14). Immunoelectron microscopic observation (15) indicated that virtually all myocytes in the affected PD-1^{-/-} hearts were surrounded by a large number of the IgG-specific immunogold particles, which were located both on the surface plasma membrane and in the extracellular matrix. In contrast, no immunogold particles were detected around the wild-type cardiomyocytes (Fig. 3B). These results suggest that IgG deposition may result from antibody binding to heart-specific surface antigens.

To confirm the presence of an autoimmune reaction against the heart, we examined mice for the presence of autoantibodies specific for heart tissue (16). Sera from all of the diseased PD-1^{-/-} mice (17 out of 17) exhibited high-titer IgG reactive to a 33-kD protein in the normal heart extract

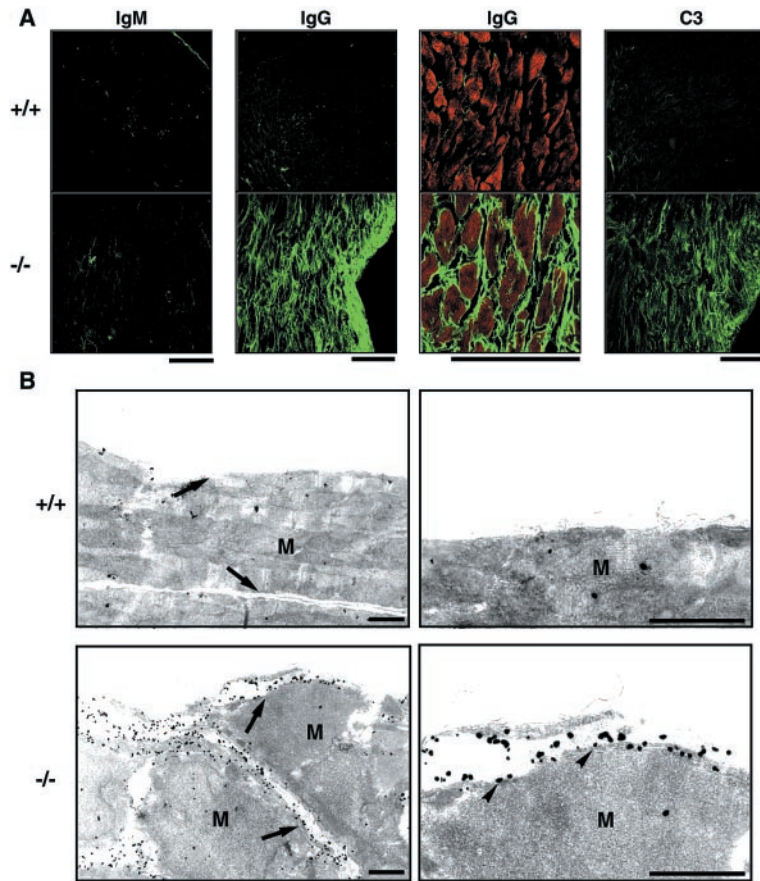
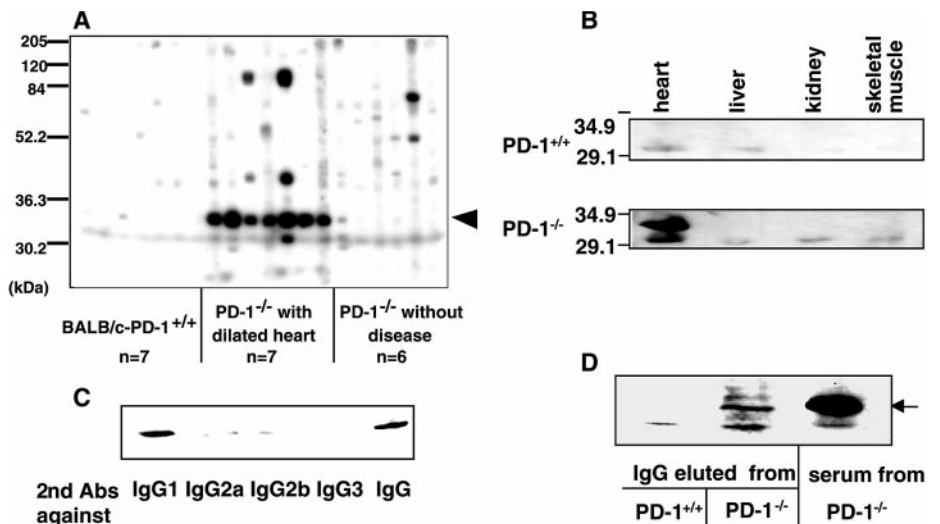


Fig. 3. (A) Deposition of IgG and C3 complement in the affected hearts of PD-1^{-/-} mice. Heart sections from PD-1^{+/+} (+/+) or PD-1^{-/-} mice (-/-) were directly stained with FITC-labeled anti-mouse IgM (left), anti-mouse IgG (middle panels), or anti-C3 complement (right). Actin was counterstained with rhodamine-phalloidin (middle right). Bars, 100 μ m. (B) Ultrastructural localization of the mouse IgG deposition around cardiomyocytes. M, myocytes. Arrow, plasma membrane; arrowhead, IgG deposition on plasma membrane. Bars, 1 μ m.

Fig. 4. Development of circulating autoantibodies against the heart tissue in diseased PD-1^{-/-} mice. (A) IgG autoantibodies were examined against the normal heart extract with sera from BALB/c-PD-1^{+/+} mice, BALB/c-PD-1^{-/-} mice with dilated hearts, and BALB/c-PD-1^{-/-} mice without the disease. Normal BALB/c heart extract was subjected to electrophoresis in 12% SDS-PAGE, blotted onto nitrocellulose filters, and probed with sera (1:300) followed by incubation with anti-mouse IgG (13). Representative results for each group are indicated. Arrowhead, 33-kD protein. (B) Immunoreactivity of sera from age-matched BALB/c-PD-1^{+/+} and BALB/c-PD-1^{-/-} mice was examined against tissue extracts of heart, liver, kidney, and skeletal muscle as in (A). (C) Isotypes of serum autoantibodies specific for the heart 33-kD antigen in PD-1^{-/-} mice. The experiments were done as in (A), except that anti-mouse IgG was used as the secondary antibody. (D) Elution of autoantibodies from the affected hearts. Heart extracts from normal BALB/c and affected PD-1^{-/-} mice were precipitated with protein G-beads; the precipitates were eluted with 0.1 M citric acid (pH 3.0), followed immediately by neutralization (3 M NaCl, 1.5 M glycine, pH 8.9). Eluate from the PD-1^{-/-} mouse contained abundant IgG relative to that from the BALB/c mouse. Immunoreactivity of the eluates was examined against normal heart extracts as in (A) along with serum from the same PD-1^{-/-} mouse.



(Fig. 4A). In contrast, autoantibodies were not detected in the sera from age-matched PD-1^{+/+} mice (0 out of 7). Similarly, sera from PD-1^{-/-} mice without macroscopic cardiomegaly did not exhibit comparable reactivity to the 33-kD protein (0 out of 21), except at very high concentrations. Reactivity was also not detected in B6 or B6-PD-1^{-/-} mice (14). Thus, the presence of high-titer IgG autoantibodies specific for the 33-kD protein in the heart correlated strongly with the clinical manifestation of dilated cardiomyopathy. The 33-kD autoantigen appeared to be specifically expressed in the heart tissue, because it was not detected in other tissues such as liver, kidney, or skeletal muscle in sera from BALB/c-PD-1^{-/-} mice with the disease (Fig. 4B).

Occasionally, we observed low but measurable titers of autoantibodies against the 33-kD protein in apparently healthy PD-1^{-/-} mice, which developed the disease within about a month. The results also suggest that autoantibodies against the 33-kD protein may be a cause of the disease rather than the result of tissue damage. No other common autoantibodies, including antibodies to double-stranded DNA, were detected in the sera of PD-1^{-/-} mice. The autoantibody was predominantly of the IgG1 subclass in all affected PD-1^{-/-} mice (7 out of 7) (Fig. 4C), consistent with the immunostaining analysis of the heart. IgG deposited in the affected heart tissue was collected by immunoprecipitation from tissue extract with protein G-beads, and by acid elution. The eluted IgG reacted to the specific 33-kD protein, which appeared to be identical to that detected in sera from diseased PD-1^{-/-} mice (Fig. 4D). These results present direct evidence that circulating autoantibodies are specifically associated with heart tissue in diseased mice. To characterize the properties of the 33-kD antigen recognized by autoantibodies, we purified the antibodies bound to the 33-kD protein and used them for staining isolated cardiomyocytes (17). Autoantibodies specific for the 33-kD protein stained the surface of cardiomyocytes with a dotted pattern that, to some extent, resembled the staining pattern observed with wheat-germ agglutinin, which binds to the transverse (T) tube (18) [Web fig. 2 (10)]. Because there are no known surface proteins of 33 kD on cardiac muscle, it is premature to conclude that the 33-kD antigen is associated with the T tube. However, it is reasonable to speculate that this protein is involved in cardiac function and that inhibition of such functional molecule by antibody binding might cause dys-

function of cardiac muscle.

Engagement of the PD-1 receptor with its membrane-bound ligand (PD-L1) of the B7 family has recently been shown to inhibit the proliferation of anti-CD3-stimulated T cells as well as anti-IgM-stimulated B cells (14, 19), indicating that PD-1 is a negative immuno-regulator of activated lymphocytes. Unlike other B7-related members, PD-L1 is detected not only in antigen-presenting cells, but also constitutively in the heart and kidney (14, 19). Thus, it is possible that cells in the heart can directly down-regulate the proliferation of autoreactive lymphocytes, ensuring a final safeguard against autoreactivity within peripheral tissues (20). Because B6-PD-1^{-/-} mice show distinct autoimmune symptoms from those seen in BALB/c-PD-1^{-/-} mice (8), the present results reinforce the notion that dysfunction of PD-1 may underlie distinct types of autoimmune diseases, which are dependent on other background genetic factors.

Dilated cardiomyopathy is a progressive and life-threatening disease, and little effective therapy is currently available. The results presented here raise the possibility that some forms of cardiomyopathy may have an autoimmune basis, and identification of possible autoantigen(s) may open new therapeutic approaches for this significant disease.

References and Notes

1. P. Richardson et al., *Circulation* **93**, 841 (1996).
2. A. Matsumori, *Jpn. Circ. J.* **61**, 275 (1997).
3. J. D. Hosenpud, J. A. Jarcho, in *Congestive Heart Failure*, J. D. Hosenpud, B. H. Greenberg, Eds. (Lippincott William & Wilkins, Philadelphia, ed. 2, 2000), p. 281.
4. A. L. P. Caforio et al., *Lancet* **344**, 773 (1994); Y. Magnusson et al., *J. Clin. Invest.* **86**, 1658 (1990).
5. K. Schulze, B. F. Becker, H. P. Schultheiss, *Circ. Res.* **64**, 179 (1989).
6. R. Klein, B. Maisch, K. Kochsiek, P. A. Berg, *Clin. Exp. Immunol.* **58**, 283 (1984).
7. To generate BALB/c-PD-1^{-/-} mice, B6-PD-1^{-/-} mice (8, 21) were backcrossed into BALB/c mice for at least 10 generations. These mice were raised in our specific pathogen-free facilities.
8. H. Nishimura, M. Nose, H. Hiai, N. Minato, T. Honjo, *Immunity* **11**, 141 (1999).
9. Hematoxylin and eosin staining was done by a standard method (8). For immunofluorescence staining, 6- to 8- μ m sections of tissues embedded in OCT compound (Miles, Elkhart, IN) were fixed with 4% paraformaldehyde-phosphate-buffered saline and stained with biotinylated F(ab')₂ fragment of goat antibody to mouse IgM, IgG (Southern Biotechnology, Birmingham, AL), or C3 complement (Cappel, Durham, NC) followed by incubation with fluorescein isothiocyanate (FITC)-conjugated streptavidin (DAKO, A/S, Denmark). Images were obtained with the laser-scanning confocal image system MRC-1024 (Bio-Rad, Hercules, CA). For transmission electron microscopy, the heart was fixed with Karnovsky solution and 1% osmium tetroxide. Polybed (Polyscience, PA)-embedded sections were stained with saturated uranyl acetate and lead citrate and observed under a JEM-1200EX electron microscope (JEOL, Tokyo, Japan) at 100 kV.

10. Supplementary data are available on Science Online at www.sciencemag.org/cgi/content/full/291/5502/319/DC1.
11. Mice were anesthetized with ketamine (50 mg/kg) and xylazine (2.5 mg/kg), and transthoracic echocardiography was performed with a cardiac ultrasound recorder (Toshiba Power Vision, Tokyo, Japan) with a 7.5-MHz transducer. After the acquisition of high-quality two-dimensional (2D) images, 1D images with time in the horizontal axis (M-mode) of the left ventricles were recorded. Measurements of left ventricular end-diastolic (LVd) and end-systolic (LVds) internal dimensions were performed by the leading edge-to-leading edge convention adopted by the American Society of Echocardiography (22). Left ventricular percent fractional shortening (%FS) was calculated as $\%FS = [(LVd - LVds)/LVd] \times 100$.
12. J. Chen, K. R. Chien, *J. Clin. Invest.* **103**, 1483 (1999); J. A. Towbin, *Curr. Opin. Cell Biol.* **10**, 131 (1998).
13. Splenocytes and bone marrow cells from 12-week-old affected PD-1^{-/-} mice were transferred intravenously into three and two BALB/c RAG-2^{-/-} mice (2×10^7 cells per mouse), respectively. Sixteen to 18 weeks after the single injection, two mice (one from each group) developed eyeball protrusion and typical dilated cardiomyopathy, as revealed by autopsy. Immunoblotting with sera of these mice demonstrated the presence of IgG autoantibodies against the heart 33-kD protein at over 1000-fold dilution.
14. H. Nishimura et al., unpublished data.
15. Immunoelectron microscopy with the pre-embedding silver-enhancement technique was done as described [A. Mizoguchi et al., *Biochem. Biophys. Res. Commun.* **202**, 1235 (1994)].
16. Normal heart extracts were prepared with a Polytron homogenizer in lysis buffer [150 mM NaCl, 25 mM tris-HCl (pH 7.4), 5 mM EDTA, 1% NP40, protease inhibitors]. Lysates were subjected to electrophoresis in 12.5% SDS-polyacrylamide gel electrophoresis (PAGE), transferred onto Hybond-ECL filters (Amersham Pharmacia Biotech, Uppsala, Sweden), and incubated with diluted sera, followed by detection with biotinylated anti-mouse IgG and streptavidin-horse radish peroxidase. Sera were diluted serially from 1:30 to 1:3000. Autoantibodies against a 33-kD protein were detected in all sera from the diseased PD-1^{-/-} mice at a 1:300 dilution, and in the vast majority of sera at dilutions >1:1000, whereas autoantibodies from the sera of PD-1^{+/+} mice were not detected even at a 1:30 dilution. In macroscopically normal PD-1^{-/-} mice and in a portion of PD-1^{+/+} mice, the autoantibodies could be detected at a dilution of 1:30 but not at dilutions \geq 1:300. The same analysis was done with 7.5% SDS-PAGE to detect higher molecular weight proteins, but no signal above background was obtained.
17. Antibodies to the 33-kD protein were affinity-purified as described [J. Sambrook, E. F. Fritsch, T. Maniatis, *Molecular Cloning. A Laboratory Manual* (Cold Spring Harbor Laboratory Press, Cold Spring Harbor, NY, ed. 2, 1989)].
18. F. Sedarat et al., *Am. J. Physiol. Heart Circ. Physiol.* **279**, H202 (2000).
19. G. J. Freeman et al., *J. Exp. Med.* **192**, 1027 (2000).
20. S. Fagarasan, T. Honjo, *Science* **290**, 89 (2000).
21. H. Nishimura, T. Nakano, N. Minato, T. Honjo, *Int. Immunol.* **10**, 1563 (1998).
22. D. J. Sahn, A. DeMaria, J. Kisslo, A. Weyman, *Circulation* **58**, 1072 (1978).
23. We thank H. Ishikawa, T. Mitsuiye, M. Hattori, E. K. Nishimura, Y. Tabuchi, and T. Toyoshima for technical comments and support and R. Yamasaki for preparation of the manuscript. Supported by grants from the Ministry of Education, Science, Sports and Culture of Japan (Center of Excellence).

16 August 2000; accepted 11 December 2000